Article

Peptide-decorated nanofibrous niche augments in vitro directed osteogenic conversion of human pluripotent stem cells

Yi Deng, Yuanyi Yang, and Shicheng Wei

Biomacromolecules, **Just Accepted Manuscript** • DOI: 10.1021/acs.biomac.6b01748 • Publication Date (Web): 09 Jan 2017

Peptide-decorated nanofibrous niche augments *in vitro* directed osteogenic conversion of human pluripotent stem cells

Yi Deng[1], *Yuanyi Yang*[4], *Shicheng Wei*[2,3,*]

[1] School of Chemical Engineering, Sichuan University, Chengdu 610065, China

[2] Department of Oral and Maxillofacial Surgery, School and Hospital of Stomatology, Peking University, Beijing 100081, China

[3] Center for Biomedical Materials and Tissue Engineering, Academy for Advanced Interdisciplinary Studies, Peking University, Beijing 100081, China

[4] Department of Materials Engineering, Sichuan College of Architectural Technology, Deyang 618000 China

ABSTRACT: Realization of clinical potential of human pluripotent stem cells (hPSCs) in bone regenerative medicine requires development of simple and safe biomaterials for expansion of hPSCs followed by directing their lineage commitment to osteoblasts. In the present study, a chemically defined peptide-decorated polycaprolactone (PCL) nanofibrous microenvironment was prepared through electrospinning technology and subsequent conjugation with vitronectin peptide to promote the culture and osteogenic potential of hPSCs *in vitro*. The results indicated that hPSCs successfully proliferated and maintained their pluripotency on the biointerface of peptide-conjugated nanofibers without Matrigel under defined conditions. Moreover, the prepared niche exhibited an appealing ability in promoting directed differentiation of hPSCs to osteoblastic phenotype without embryoid body formation step, determined from the cell morphological alteration, alkaline phosphate activity, and osteogenesis-related gene expression, as well as protein production. Such well-defined, xeno-free and safe nanofiber scaffolds that allow the survival and facilitate osteo-differentiation of hPSCs provide a novel platform for hPSCs differentiation *via* cell-nanofiber interplay, and possess great value in accelerating the translational perspectives of hPSCs in bone tissue engineering.

KEYWORDS: Peptide, polycaprolactone, nanofiber, human pluripotent stem cells, osteogenic.

1. INTRODUCTION

In contrast to adult stem cells, human pluripotent stem cells (hPSCs), including human embryonic stem cells (hESCs) and human induced pluripotent stem cells (hiPSCs), possess the remarkable capacity to self-renew and give rise to all major lineages of somatic cells, therefore, they have become promising candidates for regenerative medicine and tissue engineering application.[1, 2] Compared with hESCs, hiPSCs originated from human autologous cells circumvent the concerns regarding ethical issues and immune properties, making them ideal seed cells for regenerative medicine.[3, 4] Generally, hPSCs are cultured and differentiated on Matrigel that extracted from Engerbreth-Holm-Swarm (EHS) mouse sarcomas containing not only basement membrane components, but also plentiful inhibitors, growth factors, and a broad variety of unknown proteins, which brought about problems associated with microbial/viral contamination, immunogenicity, and variability of experimental results.[5-7] Progress in engineering chemically defined microenvironment for proliferation and osteogenic commitment of hPSCs is stringently needed for their clinical bone regenerative applications. Up to now, many natural and recombinant extracellular matrix (ECM) proteins and their fragments, such as vitronectin,[8] laminin,[9] and collagen,[10] have been exploited to maintain the self-renewal of hPSCs. Nevertheless, the significant quality variance from lot-to-lot and high cost for large scale cultivating of hPSCs resides in these biological matrices. Additionally, in terms of bone regenerative therapies, despite of the advantages that hPSCs offer, controlling their differentiation into targeted bone cells still remains a tough challenge. Hence, much effort should be made in developing economical and easily fabricated safe surfaces for multiplication of hPSCs followed by hastening their osteogenic differentiation and maturation.[11, 12]

Currently, several three-dimensional (3D) nanofibrous scaffolds made from synthetic and natural polymers have been constructed for modulating growth and improving osteogenic outcome of hPSCs consideration for the following reasons: (1) the topological structure and biomechanical performance of 3D nanofibers are akin to native ECM;[13, 14] (2) 3D nanofiber microenvironment enables to expedite the osteogenic conservation of stem cells.[15-17] For instance, a poly(l-lactic acid)/poly-benzyl-l-glutamate/collagen (PLLA/PBLG/Col) ternary nanofibrous scaffolds were fabricated by eletrospining and were proved by Ramakrishnaa et al. to promote greater osteogenic differentiation of adipose derived stem cells (ADSC) in the absence of an induction medium as evident from the enzyme activity and mineralization profiles for bone tissue engineering.[17] Ardeshirylajimi et al. found that nanofiber-based polyethersulfone (PES) scaffold could efficiently enhance the differentiation of embryoid bodies (EBs) generated from hiPSCs into osteoblastic lineage than tissue culture plastic in osteogenic inducing medium.[16] (3) After osteogenic differentiation, 3D fibrous surfaces are reported to promote the osteoblastic maturation and retain the celluar functions of osteoblasts.[18] Most of these studies, however, always use Matrigel to pretreat nanofiber surfaces for helping hPSCs attachment and proliferation. Furthermore, osteogenic differentiation of hPSCs on biomaterials usually involves the EB formation step[19-22] making it difficult to elucidate the direct interrelation between biomaterials and hPSC differentiation. To the best of our knowledge, no study has been reported on the effect of nanofibrous scaffolds on the osteogenic differentiation of hPSCs without the induction of differentiation by EB formation. Polycaprolactone (PCL), a USA Food and Drug Administration (FDA) approved material, is widely employed in bone tissue engineering due to its bioresorbability, excellent biocompatibility as well as sound mechanical properties.[23] A synthetic RGD oligopeptide derived from vitronectin (VN) protein, one component of ECM, is

proved to support the adhesion and successful self-renewal of hESCs and hPSCs for > successive 20 passages.[6, 24] In order to graft VN peptide onto PCL nanofibrous meshes through standard NHS/EDC chemistry, carboxymethyl chitosan, a natural linear amino-polysaccharide, containing a large number of amine and carboxyl groups was coated onto the electrospun nanofiber surface. With nonimmunogenicity, biodegradability, good biocompatibility, and intrinsic antibacterial properties, carboxymethyl chitosan (CMC) finds a wide range of applications in biomedical field.[25, 26] Simultaneously, it is also reported that CMC, the structural similarity to glycosaminoglycans, enables to induce osteogenic differentiation of cells.[27, 28] Herein, based on these considerations, the resultant peptide-decorated nanofibrous niche was prepared and evaluated for its role in supporting proliferation and stimulating osteo-differentiation of hPSCs under defined biointerface for the first time. We believe that the work will help greatly accelerate the introduction of hPSCs into bone repairing clinical applications cultivated in the chemically defined and safe substrate.

2. MATERIALS AND METHODS

2.1. Materials

Polycaprolactone (PCL, *Mw*≈ 80000 g/mol) was provided by Sigma-Aldrich (St. Louis, USA), and phosphate buffered saline (PBS) was obtained from ZSGB-Bio Ltd. (Beijing, China). N-(3-(Dimethylamino)propyl)-N'-ethylcarbodiimide hydrochloride (EDC), N-hydroxysuccinimide (NHS), 2-(N-morpho)ethanesulfonic acid (MES), 1,1,1,3,3,3-Hexafluoro-2-propanol (HFIP), and carboxymethyl chitosan (CMC, *Mw*≈ 9.5-20.9 kDa, degree of carboxymethyl substitution≥ 86 %) were purchased from Aladdin (Shanghai, China). To facilitate chemical conjugation onto the material surface, the peptide was modified at its N-

terminal with a lysine-containing spacer. Vitronectin (VN) peptide [Ac-KGGPQVTRGDVFTMP sequence], supplied from Chinapeptides Co., Ltd. (Shanghai, China), were synthesized by a batchwise fmoc-poly-amide method and had more than 98 % purity per the high-pressure liquid chromatography profile. The primary antibodies including rabbit monoclonal antihuman Oct-4, rabbit monoclonal antihuman SSEA-3, mouse monoclonal antihuman Tra-1-60, mouse monoclonal antihuman Nanog, mouse monoclonal antihuman SSEA-4, rabbit monoclonal antihuman Runx2, rabbit monoclonal antihuman Col1a1, mouse monoclonal antihuman OPN, and mouse monoclonal antihuman OCN, were all purchased from Cell Signaling Technology (USA). All other chemicals were of analytical reagent grade, and all aqueous solutions were prepared with deionized water (D.I. water).

2.2. Preparation of electrospun PCL nanofibers

PCL was first dissolved in HFIP at a concentration of 10 % (w/v, PCL/HFIP) by ultrasonic and vigorous stirring overnight to obtain a homogenous solution. Afterwards, the solution was placed into a syringe with a stainless-steel blunt needle (23 G) whose inner diameter is 0.5 mm. Electrospinning of PCL nanofibers was carried out using a commercial electrospinning equipment (SS-2535, YongKang Technology Co., Ltd., China) with a rotating collector covered with Al foil. The electrospinning parameters were set at the applied voltage of 15 kV, the collection distance of 10 cm, and the feed rate of 1.0 mL/h. The as-prepared electrospun fibrous meshes were vacuum-dried at room temperature to remove residual organic solvent for future use.

2.3. Immobilization of CMC and peptide on the surface of nanofibers

After being thoroughly washed, the samples were immersed in 3 w/v% CMC solution for 24 h at 37 °C in a constant-temperature shaker (ZWY-103B, Shanghai ZHICHENG

Analytical Instrument Manufacturing Co., Ltd.), and then the treated samples were thoroughly rinsed to remove the physically-absorbed CMC, which were named as CMC-PCL. To conjugate VN peptide on the surface, the PCL-CMC samples were firstly pretreated by 2 mM EDC and 5 mM NHS in 0.1 M MES buffer (pH= 5.6) for 40 min. Then, VN peptide solution (1 mM, dissolved in sterile PBS buffer) was incubated onto the carboxyl-rich CMC-grafted PCL nanofiber in 4 °C refrigerator for another 24 h. The resulting peptide-decorated nanofibrous scaffolds (denoted as pep-CMC-PCL) were thoroughly washed by D.I. water and dried under nitrogen influx before characterization and cell experiment. VN-decorated glass slides (named as pep-CMC-glass) were also prepared in the light of the same process as control group.

2.4. Surface characterization

Fourier transform infrared with attenuated total reflection (ATR-FT-IR) spectra (Magna-IR 750, Nicolet, USA) were collected to analyze the functional groups of the products in the range of 400 cm^{-1} to 4000 cm^{-1}.

The surface hydrophilicity was determined by a contact angle goniometry (SL200B, Kino, Norcross, USA) equipped with a high-resolution camera based on the sessile drop method using 2 mL of D.I. water droplets under ambient temperature and humidity. Surface energy was further calculated by the matching software from Kino Industry (http://www.uskino.com/article/65.html). Measurements were taken until droplets were well settled on samples and repeated in triplicate, at six different positions per substrate type.

Surface topologies of the various treated substrates were characterized by a field emission scanning electron microscope (FE-SEM, JSM-6701F, JEOL, Japan) at an accelerating voltage of 20 kV. All samples were coated by gold for 30 s before SEM observation.

Atomic force microscopy (AFM, Dimension ICON, Bruker) was employed in contact modes (a Si_3N_4 cantilever with a spring constant of 0.12 N/m) in dry condition to assess morphological characteristics of the bare and modified PCL substrates. Surface roughness including arithmetic average roughness (Ra) and root mean square roughness (Rq) were also calculated from the roughness profile, and each sample was tested in sextuplicate to improve the statistics.

The alteration of chemical constituents and elemental states of the different PCL samples were analyzed by X-ray photoelectron spectroscopy (XPS, Kratos Analytical Ltd., Manchester, UK) for both survey and high-resolution spectra. The binding energies were calibrated by the C 1s hydrocarbon peak at ~285 eV. Besides, the quantitative analysis and curve fitting were conducted using the CasaXPS software package.

To know whether the peptide was grafted onto the nanofiber surface or not, the FITC-labeled VN peptide (FITC-VN) was applied to anchor onto the active CMC-PCL substrate through NHS/EDC chemistry in 4 °C for 24 h. Afterward, samples were rinsed with PBS and captured under laser scanning confocal microscope (LSCM, Carl Zeiss, Germany) to visualize the attached peptide at 488 nm excitation wavelength and 525 nm emission wavelength.

2.5. Cell culture and seeding

The hiPSCs (hNF-C1 line, provided by Chinese Academy of Sciences, GIBH, Guangzhou, China) were generated from dermal fibroblasts by retroviral introduction of four Yamanaka's factors: Oct3/4, Sox2, Klf4 and c-Myc. The hESCs (H9 line, supplied from GIBH) from the inner cell mass (ICM) of blastocyst-stage embryos were also used in the present study. Matrigel (BD Biosciences, Canada) was diluted with Dulbecco's modified eagle medium/F12 (DMEM/F12, Gibco, USA) at a ratio of 1:160 at 4 °C. Two sorts of hPSCs were cultured on Matrigel-coated plates using chemically defined mTeSR^{TM}1 medium (StemCell Technologies,

Canada) containing 10 μM Rock inhibitor (Y-27632, Selleck Chemicals, USA), and 1 v/v% penicillin/streptomycin (Invitrogen, USA) at 37 °C in a humidified 5 % (v/v) CO_2 incubator (MCO-18AIC, Japan). Cells between 30-50 times of passages were used for the *in vitro* experiments. Cells were fed daily and passaged at 1:3 splitting ratio every 3-4 days by exposure to EDTA (Aladdin, Shanghai, China) at 0.125 wt/v% for 5.5 min. Prior to cell experiments, the prepared meshes were cut into round shape and sterilized with 75 % ethanol for 1 h, followed by thorough rinse with disinfected PBS buffer. When reaching 70-75 % confluence, cells were dissociated with EDTA, counted and seeded onto fibrous scaffolds at a density of 1.6×10^5 cells per mL.

2.6. Cell growth and pluripotency

2.6.1. Cell proliferation assay

Cell viability of hiPSCs and hESCs on samples was evaluated using cell counting assay kit-8 (CCK-8, Dojindo Laboratories, Kumamoto, Japan) following the manufacturer's protocol. At desired time intervals (12 h, and 1 day-5 days) of cultivation, CCK-8 solution was added into each well at a proportion of 1:10 (v/v) for 2 h incubation in the dark. Then 100 μL of supernatant from each well was transferred to new 96-well cell culture plates using a pipette. The absorbance value of the supernatant optical density (OD value) for each group was measured with a microplate reader (model 680, Bio-Rad, Canada) at 450 nm wavelength with a reference wavelength of 630 nm. hPSCs cultured on pep-CMC-glass were served as control group. Six parallel specimens were used to provide an average and standard deviation.

2.6.2. SEM observation of cells

The typical cellular morphology on the fibrous scaffold in mTeSR^{TM}1 was evaluated by FE-SEM (JSM-6701F). Basically, after 1 and 3, 5 days incubation, the samples with cells were

taken from culture plates, rinsed with PBS buffer and fixed in 2.5% glutaraldehyde solution for 30 min, followed by dehydration with graded ethanol solutions (50 %, 70 %, 80 %, 90 %, 95 %, and 100 %, 10 min each concentration) and dried for SEM observation (JSM-6701F).

2.6.3. Cell pluripotency test

Both hiPSCs and hESCs were cultured on peptide-decorated nanofibers in 24-well plates for 1 day and 3 days, respectively. The hPSCs before osteoinductive differentiation surface were subjected to immunofluorescence analysis. They were fixed with 4% (v/v) paraformaldehyde for 15 min and permeabilized with 0.1% (v/v) Triton X-100 (Solarbio, Beijing, China) for 10 min at room temperature. Afterward, they were incubated with 1 % bovine serum albumin/PBS buffer at 37 °C for 30 min to block nonspecific binding. Then, cells were incubated with diluent primary antibodies Oct-4 (1:1000 dilution), SSEA-3 (1:400 dilution), and SSEA-4 (1:400 dilution), and Tra-1-60 (1:200 dilution) at 4 °C overnight. After incubation with primary antibodies, cells were washed thrice with PBS and incubated for 1 h at room temperature with FITC-488 goat antirabbit (1:100, XSGB-BIO) and TRITC-543 goat antimouse (1:100, XSGB-BIO) secondary antibodies. All staining steps were followed by three washes in PBS buffer. Fluorescence signals were viewed immediately under LSCM (Carl Zeiss).

2.7. Osteogenic induction

Osteoinductive medium comprised fresh low-glucose DMEM containing 10% fetal bovine serum (FBS, Gibco, Carlsbad, Canada), 100 U/mL penicillin, and 100 mg/mL streptomycin (Invitrogen), 50 μg/mL ascorbic acid, 10 mM sodium β-glycerophosphate, and 100 nM dexamethasone. The hPSCs were first attached to the nanofibrous substrates in mTeSR^{TM}1 medium for 2 day. Afterward, the culture medium was replaced by osteoinductive medium. The culture medium was refreshed every 2-3 days, and the whole process lasted for 28 days. Day 1

was referred to the day when osteogenic induction commenced, and Day 0 denoted the time when cell before osteogenic stimulus.

2.8. Osteogenic differentiation

2.8.1. Cell morphology observation

Cellular morphology and spreading of hPSCs after osteogenic induction on samples were also evaluated using SEM. After different induction time (Day 0, 2, 7, 14, and 28), the scaffolds with cells were fixed in 2.5% glutaraldehyde solution, dehydrated with graded ethanol solutions, and dried for SEM observation (JSM-6701F).

2.8.2. Alkaline phosphatase (ALP) activity

ALP activity of hiPSCs and hESCs on samples was carried out by an ALP assay reagent kit (Nanjing Jiancheng Bioengineering Institute, China) following the manufacturer's instruction. A 1 mL cell suspension was seeded on peptide-decorated nanofibrous niche and peptide-decorated glass slides at a density of 1.6×10^5cells/mL in 24 well-plate. After Day 0, 4, 7, 14, and 21 of osteoinduction, the supernatant was removed and 100 μL of lysis solution (1% TritonX-100) was added into each well and incubated for 1 h. After that, 30 μL of resulting cell lysates at each well was transferred to new 96-well cell culture dishes, and cultivated with 50 μL of carbonated buffer solution (pH= 10) and 50 μL of substrate solution (4-amino-antipyrine) at 37 °C for 15 min. Then 150 μL of potassium ferricyanide (chromogenic agent) was added into the mixed solution and the production of *p*-nitrophenol was determined by the absorbance at 520 nm on a microplate reader (Elx-800, Bio-Tek Instruments, USA). For normalization, the total protein concentration was measured using a bicinchoninic acid (BCA) protein assay kit (Thermo, USA). Thus, ALP activity was normalized and expressed as the total protein content (U/g of prot). Six specimens were tested for each incubation period.

Meanwhile, enzyme-histochemistry (EHC) staining was also performed to visualize ALP distribution and expression on sample surface at the same time points using a BCIP/NBT ALP color development kit (Beijing ComWin Biotech, China).

2.8.3. RNA extraction and quantitative real-time PCR

After Day 7, 14, and 21 of osteoinduction, the total mRNA was isolated from cells using TRIzol (Invitrogen, USA) and reverse transcribed into cDNA using a Revert Aid First Strand cDNA Synthesis Kit (Thermo, USA) as per the manufacturer's instruction. Then, quantitative real-time polymerase chain reaction (RT-PCR) analysis was conducted with SYBR SYBR Green (Roche, USA) on an ABI 7500 RT-PCR machine (Applied Biosystems, USA). All were performed in triplicate and the expression of glyceraldehyde-3-phosphate dehydrogenase (GAPDH) was employed as house keeping gene. Primers (provided from Sangon Biotech, Shanghai, China) used in the present study were listed in Table S1. Primer sets (10 mM final concentration for each primer) were used in a volume of 20 mL per tube. The thermal profile of the PCR was 50 °C for 2 min and 95 °C for 10 min, followed by 40 cycles at 95 °C for 5 s and 60 °C for 1 min. The cycle threshold values (Ct values) were applied to determine the fold differences by ΔΔCt method.

2.8.4. Immunofluorescence

After different days (Day 7, 14, 21) of osteogenic stimulus, cells on samples were fixed with 4 % paraformaldehyde, permeabilized with 0.1 % Triton X-100. After rinsing with PBS, cells were incubated with 1 % BSA/PBS buffer to block nonspecific binding. Then, cells were incubated with osteogenesis-related primary antibodies Runx2 (1:400 dilution), Col1a1 (1:400), Nanog (1:400 dilution), OPN (1:400 dilution), and OCN (1:400 dilution) at 4 °C overnight. The next day, cells were incubated with secondary antibody (1:100, XSGB-BIO) at a dilution of 1:100 for

1 h in the dark at ambient temperature. Furthermore, the cytoskeleton was stained with 5 μg/mL FITC-phalloidin (Sigma-Aldrich) for 30 min. The fluorescence signals in the cells were observed by a LSCM (Carl Zeiss).

2.9. Statistical analysis

All the quantitative data were expressed as mean ± standard deviation. Statistical analysis was done using SPSS 10.0 software. One-way analysis of variance (ANOVA) or Student's t-test was used to determine the significant differences among the groups, and *p*-values less than 0.05 were considered statistically significant.

3. RESULTS AND DISCUSSION

3.1. Surface composition and morphology of peptide-decorated nanofibers

In this study, a facile biomimetic method was applied to develop a 3D peptide-decorated niche with the functions in supporting growth and boosting the osteogenic conversion of hPSCs *in vitro* as schemed in Fig. 1. Briefly, the PCL nanofibers were prepared through traditional electrospinning technology. To better immobilize peptide, CMC molecule as a bridge (intermediate layer) was further grafted to the nanofibrous surface. The -COOH groups on the resultant CMC-PCL surfaces were preactivated with the NHS/EDC chemistry to facilitate the VN peptide tethering of terminal carboxyl groups to the NHS groups, producing peptide tethering surfaces for culture of hPSCs without Matrigel and EB formation step.

To explore the alteration of chemical composition and morphology after different stages of surface functionalization, the modified PCL nanofibrous meshes were characterized by FT-IR, contact angle goniometry, XPS analysis and AFM, as well as SEM. The ATR-FT-IR spectra of the functionalized samples were shown in Fig. 2a. The bands detected at 2866 cm^{-1} and

2944 cm^{-1} were corresponded to the characteristic absorption of C-H stretching vibrations. The absorption band at approximately 1165 cm^{-1} and 1241 cm^{-1} was putatively assigned to the symmetric and asymmetric stretching vibration of C-O-C in PCL.[29] The strong peak at 1723 cm^{-1} were associated with C=O stretching bonds. These are the characteristic peaks of pure PCL. After CMC modification, nonetheless, the new peaks at 1648 cm^{-1} and 1555 cm^{-1} obviously showed up, which should be associated with the C=O stretching vibration of amide I (νC=O) and the deforming vibration of amide II (δN-H) of CMC.[30] The typical broad peaks of hydroxy group (OH^-) were observed at about 3378 cm^{-1}. In addition, the intensity of the three peaks was enhanced which might result from the superimposed vibration of amido bond and hydroxy group after introducing peptide onto CMC-PCL surface, suggesting that VN peptide was effectively covalently bonded on CMC-grafted PCL nanofibers. The water contact angle on a substrate has been extensively used to track and evaluate the effectiveness of surface modification protocols. High contact angle values describe hydrophobicity, and low angles indicate hydrophilicity. Initially, the bare PCL nanofiber was super-hydrophobic (122.3 ± 3.91 °), corresponding to the lowest surface free energy (17.52 ± 0.97 mJ/m^2) among them. The water contact angle on the nanofiber after CMC anchoring dramatically decreased by about 82 °, due to the hydrophilic groups (-OH, -NH-C=O, and $-NH_2$) of the grafted CMC on the hydrophobic PCL surfaces. Additionally, immobilization of the peptide onto the CMC-coated PCL nanofiber continuously reduced the water contact angle to 23.8 ± 1.0 ° (surface free energy= 66.1 ± 2.1 mJ/m^2) in Fig. 2b, attributing to the hydrophilic nature of peptide, which implied that VN peptide was successfully grafted onto the PCL nanofiber *via* CMC interlayer. It is recognized that, in biological systems, hydrophilic biointerface of implant is capable of promoting the adhesion and

proliferation of cells *via* increasing the adsorption of essential proteins in the cell culture media.[31, 32]

These findings were further verified by an XPS survey scan (Fig. 3, and Table S2). In the full scan spectrum of pristine PCL nanofibers, carbon and oxygen elements were the predominant components. Successful anchoring of CMC was indicated by an increase in the N 1s and O 1s content, and a corresponding decrease in the C 1s content from 78.29 % to 69.03 % as shown in Table S2. Upon attachment of peptide on the surface, notably in the wide-scan spectra, the appearance of a sodium signal (because the peptide was dissolved in PBS buffer), and the enhancement of nitrogen peaks (N 1s, from 2.26 % to 3.03 %) on the surface of pep-CMC-PCL samples indicated successful tethering of VN peptide. Furthermore, an evident change in the carbon bond composition observed in the high-resolution narrow carbon spectra (C 1s) clearly supported these conclusions (Fig. 3b-d). The high-resolution C 1s spectrum of the pristine PCL was deconvoluted into three different curves. The binding energies centered at 284.6 eV, 286.1 eV and 288.7 eV could be assigned to the -C-C-/-C-H-, -C-OH, and -C=O bonds, respectively. After CMC coating, the intensity of the carbon skeleton (-C-C-/-C-H-) decreased dramatically from 52.91 % to 41.05 %, and the peaks of the hydroxyl (-C-OH) and carbonyl (C=O) groups increased as shown in Fig. 3c. This should be attributed to the ample hydrophilic groups of CMC. Whereas a broad peak of the -C-N- bond at about 285.3 eV was newly recorded on both CMC-PCL and pep-CMC-PCL samples, indicating the presence of CMC and peptide. Compared with that of CMC-PCL, the peaks of -C-N- and C=O for peptide-conjugated samples were enhanced greatly in intensity due to the abundant presence of amine groups and amide bonds (-NH-C=O) in the structure of VN peptide molecule, which further proved the successful peptide tethering. Furthermore, by fitting the distribution of the

high-resolution N 1s spectra of CMC-coated and peptide-tethered PCL using Gaussian/Lorenz curve, three peaks were obtained for both of them (Fig. S1). The peaks centered at 399.4 eV, 400.3 eV, and 401.5 eV were consistent with the protonated amine specie ($R\text{-}NH_3^+$), amide (-NH-C=O), and amine bond ($R\text{-}NH_2$), respectively. We could see that the content of -NH-C=O component in the total of N 1s line increased accompanied with the reduction of $R\text{-}NH_2$ and $R\text{-}NH_3^+$ in the spectrum of pep-CMC-PCL sample, which might ascribe to the covalent bonding formation between the negative COO^- group of CS and the $R\text{-}NH_2$ group of peptide. More visually, under LSCM (Fig. S2), green fluorescent nanofibrous network structures were observed when it modification with FITC-labeled peptide, further corroborating the loading of VN peptide on the surface of PCL nanofibers. These results obviously indicated that peptide was easily immobilized on the CMC-functionalized PCL surface.

PCL nanofiber with immobilized CMC and peptide were analyzed by SEM and AFM to investigate surface topology and roughness. As presented in Fig. 4, the pure PCL electrospun meshes possessed a uniform and smooth surface morphology with the diameter of 2.56 ± 0.07 μm. The introduction of CMC, nevertheless, made the fibrous surface rough, and some nodule-like structures were detected in CMC-PCL and pep-CMC-PCL fibers. Furthermore, the surface roughness including Ra and Rq were also determined by AFM. Following CMC modification, the relative roughness of CMC-PCL significantly increased from 789 ± 51 nm to 960 ± 62 nm for Ra and from 931 ± 43 nm to 1162 ± 79 nm for Rq, compared with the pristine PCL nanofibers. Addition of peptide also improved the surface roughness of the modified PCL substrates. Based on the literature evidence, an appropriate rough microtopography can promote osteoblastic conversion of hMSCs and accelerate ingrowth of soft and hard tissue into the materials.[33-35]

3.2. Cell viability

The adhesion and proliferation of the hPSCs cultured on the VN peptide-riched fibrous scaffolds and glass slides for 12 h, and 1 day-5 days were determined by CCK-8 assay. Fig. 5 showed that a conspicuous increase in the cell proliferation was detected in all materials with increasing culture time, which could be considered the good cytocompatibility of biomaterials. In accordance with earlier work, VN peptide surface could promote hPSCs attachment and proliferation *via* RGD-cell integrin interaction, and hiPSCs adhesion is significantly influenced by the peptide density on the surface.[6, 36] Compared with pep-CMC-glass group, the pep-CMC-PCL nanofibers displayed a lower vitality especially at long culture periods (3-5 days), implied that cells preferred to attach and grow on smooth two-dimensional (2D) surfaces than rough three-dimensional (3D) ones, which was in line with previous publications.[37, 38] Gao et al. cultured hMSCs on both PCL nanofibrous scaffolds and glass surfaces, and observed that more stem cells were grown on glass compared with fibrous scaffolds regardless of in serum-contained and serum-free culture media.[37] Turng also found that mouse NIH3T3 cell attachment on poly(propylene carbonate) and poly(propylene carbonate)/chitosan nanofibers was lower than that of 2D tissue culture plastics.[38] Besides, comparing the two hPSCs, more hiPSCs were attached on the peptide-tethered nanofibrous scaffolds than hESCs. Although 2D plate culture has an advantage over 3D fibrous scaffold culture regarding cell numbers, numerous literature has proved that nanofibrous surface plays an obvious promotive role on cell differentiation. Therefore, a variety of 3D nanofibers fabricated form synthetic and natural polymers were developed to manipulate and hasten the committed differentiation hPSCs to neuron/neurocyte-like,[19, 39] hepatocyte-like,[40, 41]

cardiomyocyte [42, 43], or primordial germ cells[44] and so on, but limited effort is put in investigation the role of nanofibrous surfaces in osteogenic stimulation of hPSCs.

3.3. Cell morphology and pluripotency

In general, it is quite a challenge to support attachment and growth of hPSCs without Matrigel. In order to examine the influence of the VN peptide-loaded nanofibers on the cellular morphology and pluripotency, SEM observation and immunofluorescence staining of two hPSCs were conducted. Undifferentiated hPSCs exhibited a high nucleus-to-cytoplasm ratio, formed tightly packed colonies with defined colony borders, and expressed pluripotency markers.[45, 46] The hiPSCs and hESCs were both robustly attached onto the pep-CMC-PCL nanfibrous scaffold with remarkable spreading after seeded for 24 h (Fig. 6), and maintained typical undifferentiated morphology during 5 days of culture. The SEM image showed that hPSCs incubated on peptide-decorated nanofibers grew in tightly packed colonies and defined colony borders. It was worth to note that the size of hPSCs colonies increased with the extension of time, indicating that the hPSCs could well proliferate on the peptide-decorated PCL nanofibers. By comparison, no cell adhered on "bare" PCL nanofiber surface. Maintenance of pluripotency is a critical parameter when evaluating new niches for hPSCs culture. Immunofluorescence staining was carried out to estimate whether cells retained markers of undifferentiated hPSCs. The POU family transcription factor Oct-4 is a highly specific and indispensable biomarker for undifferentiated hPSCs;[47] SSEA-4 and SSEA-3 are glycolipid cell surface antigens powerfully expressed in undifferentiated hPSCs;[45] and Tra-1-60 expressed on podocalyxin is a stem cell-defining marker found on the membrane surface of hPSCs.[48] Results revealed the strong positive staining of Oct-4, Tra-1-60, SSEA-3, and SSEA-4 in cultures of the peptide-decorated surface throughout 1 and 3 days, indicating that hiPSCs and hESCs all remained their undifferentiated characteristics very

well on the peptide-decorated substrate during 3 days of culture. At the same time, cells on the nanofibrous scaffolds exhibited the morphology most similar to undifferentiated hPSCs, as characterized by compact colonies with several cells and large nuclei-to-cytoplasm ratios as shown in Fig. 7. Spontaneous differentiation on the edges or in the center of the colonies was rarely observed on the peptide-decorated substrate. Overall, these results demonstrate that a short peptide sequence from VN protein conjugated on the PCL nanofibers could robustly support hPSCs proliferation and maintain their pluripotency under a fully defined medium (TeSR^{TM}1). Compared with Matrigel-coated nanofibers, the peptide-decorated nanofibers avoid the problems related to immunogenicity, microbial and viral contamination. Hence, our VN peptide-decorated PCL nanofibers through CMC modification may be suitable for hPSCs culture without Matrigel coating.

3.4. Osteogenic differentiation

For optimal expansion and differentiation of hPSCs in bone regenerative applications, it is much-needed to design an osteogenic environment that mimics cell niche and induces ossification of cells on chemically defined biomaterials. To evaluate whether the hiPSCs/hESCs enable being directly induced toward osteogenic lineages *in vitro*, the cellular morphological alteration, the ALP activity, and the expression of osteogenesis-related genes, as well as corresponding protein expression were assessed at specific time intervals.

3.4.1. Cell morphology alteration

Figure 8a-b presented a typical overview of hiPSCs and hESCs morphologies on sample surfaces at Day 0, 2, 7, 14, 21 and 28 under SEM, respectively. Before ostegenic stimulus, hPSCs colonies with intrinsic undifferentiated morphology were detected on the fibrous scaffolds, whilst after directed differentiation in osteincutive media, apparent change in cell

morphology were found. The cell colonies collapsed to several parts, and some differentiated cells with variable morphologies migrated from the periphery of hPSCs colonies on the peptide-decorated nanofibers, indicating that hPSCs differentiation occurred at the edges of the colonies. When time prolonged to Day 7 and Day 14, these differentiated cells possessed a low degree of cell-cell contact area existed in the form of single cell, and they displayed a highly flattened morphology with numerous filopodia, similar to osteoblastic morphology, which indicated that net-like microstructure of nanofibers provided favorable environment for cell differentiation owing to structural similarity to ECM. Moreover, at the high magnification, the presence of abundant cellular filopodia demonstrated a good adhesion and spreading of cells. During 21 days of osteoinduction, such phenomenon aggravated, however, the number of cells adhering to modified PCL nanofibers decreased at Day 28, implying the excessive induction time in osteogenic inducing media might adverse to cell growth/proliferation. The results indicated the synergistic effect of osteoblast-inducing chemical factors (including β-glycerophosphate, ascorbic acid and dexamethasone) and nanofibrous topological cue could accelerate the oesteogenic commitment of hPSCs. Meanwhile, the result also revealed that 21 days might be the optimal time for osteogenic conservation of hPSCs under osteinductive media.

3.4.2. Alkaline phosphatase activity

ALP, an early marker of osteogenesis, was expressed strongly in undifferentiated hPSCs, as well as in the osteoblasts. As shown in Fig 9a, it was evident that there were distinguished ALP expression between hiPSCs and hESCs on peptide-decorated PCL nanofibrous scaffolds. As for hiPSCs, the production of ALP increased slightly during the first four days, and then decreased to about zero after being induced for 7 days, indicating that hiPSCs began to lose their stem cell properties. Later, the expression of ALP re-increased with the extent of time and kept at a high

level (72.1 ± 6.7 U/gprot) after 14 days, which signified the appearance of osteogenic progenitors after 14 days of osteoinductive culture. Clearly, the ALP signal on VN peptide-conjugated nanofiber group reached a substantially higher level compared with that of glass group after Day 7, and the level of ALP production in the pep-CMC-PCL group was about 1.35 times than that of pep-CMC-glass sample at Day 21. With regard to hESCs, differing from that of hiPSCs, ALP expression initially sharply reduced to a low level after 4 days of ostegenic stimulation, whereafter it steadily elevated to 102.8 ± 5.6 U/gprot. The amount of ALP production on the modified fibers was 1.27-fold that of its counterpart (pep-CMC-glass) at Day 21, although there were no difference between two groups before 7 days of culture. In spite of a little different result, the similarity between two hPSCs (i.e., hESCs and hiPSCs) in promoted ALP activity was observed on the VN peptide-decorated surfaces, implying that the nanofiber might have a positive impact on the osteogenesis of hPSCs. As mentioned above, various studies have showed that nanofibrous topology serve as temporary ECM significantly influences the differentiation of various cell types as well as EBs from hPSCs.[15, 16, 49] These results were further qualitatively confirmed *via* EHC staining of ALP at Day 14 and 21 (Fig. S3), exhibiting a good time-dependent ALP expression. By comparison, the ALP-positive areas were obviously larger and darker on pep-CMC-PCL nanofibers than on pep-CMC-glass, suggesting the long-term stimulating effect of the presence of nanofibrous matrixes on hPSCs' osteo-differentiation.

3.4.3. Osteogenic biomarker expression

Cells are capable of sensing and responding to the biophysical stimuli from the surrounding microenvironment, triggering a cascade of intracellular events regulating the gene expression involved in cell fate like differentiation. An in-depth study at molecular level is helpful to

better understand the differences between 3D nanofiber-hPSCs interaction and 2D plate-hPSCs interaction. Therefore, the study revealed the typical osteo-specific genes expressions of hPSCs grown on pep-CMC-PCL and pep-CMC-glass encoding Runx2, ALP, Col1a1, and OCN (osteocalcin) assessed by quantitative real-time PCR for 7, 14 and 21 days. It is well-known that Runx2 is the early and master transcription factor initiating the osteogenic lineage transcriptional program, which contributes to up-regulation of various downstream bone-related genes such as OCN and Col1a1 *via* binding to the core site of their enhancers or promoters.[17] OCN is considered the most-characteristic indicator for mature osteoblasts and mineralization at a late stage of osteogenesis, and it accumulates and reaches the maximum amount in the calcified bone due to its high affinity for apatite crystals.[50] Col1a1 gene is an osteo-special marker encoding the pro-α 1 chains of type 1 collogen, which is an extracellular matrix and structural protein contained in the bone ECM.[50] Among these osteo-related biomarkers, ALP is a membrane-bound enzyme and plays an essential role in the early mineralization of the bone matrix through hydrolysis of organic phosphates.[51] The peak of Runx2 expression located on Day 14, in line with previous studies, because the early marker Runx2 functionalized at the prior period and began to degrade after completing its role. As shown in Fig. 10, the fold change in expression of Runx2 and ALP for hiPSCs on pep-CMC-PCL nanofibers was more than that on pep-CMC-glass groups at Day 14 and 21, however for hESCs, the higher un-regulation in Runx2 and ALP expression on pep-CMC-PCL surface were only detected at Day 14 and 21, respectively. In particular, the Col1a1 and OCN expression of mRNA when both hiPSCs and hESCs cell lines were cultivated on the pep-CMC-PCL nanofibers remarkably outmatched those on the pep-CMC-glass substrate from Day 14 to Day 21. These results showed that osteoblastic

differentiation of hPSCs strongly happened and more actively on 3D nanofibrous microenviroment than 2D culture with plate surface.

To further verify the results from gene analysis on the peptide-decorated fibrous substrates, the production of some osteogenisis-related makers including Runx2, Col1a1, OPN, and OCN, as well as cytoskeletons stained by FITC-phalloidine were also probed through immunofluorescence staining. Osteopontin (OPN), one of the most abundant non collagenous proteins of bone matrix, plays a key role in the process of bone mineralization.[52] At Day 7, hiPSCs and hESCs subjected to the nanofibers were positive for Runx2 and slightly expressed Nanog, a typical marker for an undifferentiated state of hPSCs, implying that hPSCs began to lose their stemness. As osteoinductive time proceeded to Day 14, all cells strongly expressed a production of Runx-2 marker but negative for Nanog (Fig. S4). In Fig. 11, nanofiber scaffolds were visualized to blue color at 488 nm excitation wavelength. We could see that differentiated cells attached onto the nanofibers very well, and they displayed a strong expression of bone-specific ECM proteins such as Col1a1 (green), OPN (red), and OCN (red), implying that nanofibrous structure could have an additive effect in enhancing the osteogenic conversion of hPSCs. Moreover, the cytoskeletons in cells were also stained by FITC-phalloidin after ostegenic stimulus of hPSCs on the peptide-decorated PCL fibers at Day 21. In addition to celluar morphological alteration, most differentiated cells seeded on fibrous samples exhibited favorable spreading by re-organized focal adhesions and filamentous F-actin, and by outstretching lammellipodia, that were typical behaviors of osteoblasts cultured on nanofiber surfaces reported in previous work.[53-55] Furthermore, these cells stained strongly positive for OCN, which is a biomarker for mature osteoblasts. Our current data from foregoing osteogenic differentiation experiments supported the hypothesis that the combined

employment of classical osteoinductive media and nanofibrous scaffold greatly improved the osteogenic efficiency of hPSCs, subsequently resulting in the acceleration of the osteogenesis.

As is well known, ECM is a complex mixture constituted of collagen-based nanofibrous skeleton, structural proteins (e.g. vitronectin, and fibronectin), and glycosaminoglycans (polysaccharides).[56] In the hPSCs culture niche, the oligopeptides from VN protein, a most common cell adhesion motif, undoubtedly elicits an imperative role in attachment of hPSCs. The structure of CMC is akin to glycosaminoglycans, which is documented to enhance the expression of ECM in human osteoblasts and chondrocytes and stimulate the osto-differentiation of osteoprogenitor cells.[57] On the other hand, CMC polysaccharide possesses a low elasticity modulus close to ECM, and it is proof that a soft surface is conductive to hPSCs culture.[58] Actually, in the physiological microenvironment of bone tissues, in addition to biochemical cue, the 3D fibrous structure in bone ECM also guides many cell behaviors like adhesion, migration proliferation and differentiation through providing adaptive accommodation and a complex set of mechanotransductive stimulation associated with Wnt/catenin pathway, Integrin-mediated pathway, and MAPK-dependent PPAR signaling pathway.[59, 60] Lim et al. found that the nanofiber topography itself was sufficient to regulate stem cell differentiation through promoting the activation of the Wnt signaling pathway.[59, 60] PHBHHx electrospun nanofibers were reported by Wu et al. to effectively enhance the osteogenic differentiation of MSCs *via* mediating the MAPK-dependent PPAR signaling pathway.[60] Numerous published literature has demonstrated that nanotopographic features of synthetic fibers mimic ECM exert robust influence on the osteogenic differentiation of stem cells because of their niche-mimicking features.[61, 62] Another important evidence from Deng and his co-workers is that the in-depth pathway analysis revealed that focal adhesion kinase, Wnt, TGF-β, and MAPK pathways were

collectively involved in the activation of osteogenic differentiation in human bone marrow mesenchyme stem cell (hBMSCs) on poly-l-lactide (PLLA) nanofibers.[63] However, they also found that the extent of osteogenic differentiation on the fibrous scaffold was much lower but similar rhythm of dynamic cellular behavior compared with that driven induced by chemical osteogenic supplements, demonstrating that mechanotransduction from nanofibrous scaffolds might trigger nonspecific and multilevel activation of osteogenic differentiation in stem cells. [63]

Several previous reports have shown that nanofibrous scaffold containing poly(ether sulfone) (PES), and poly(L-lactic acid) (PLLA))[16, 64] provide help to promote the osteogenic conversion of hPSCs through EBs formation. EBs are commonly adopted for hPSCs' differentiation because they mimic the three dimensionality of development during gastrulation and formation of the three germ layers *in vivo*. Nevertheless, the limitation of employing EBs for differentiation studies arises from the fact that the yield of desired cells is much lower than the initial amounts of cells.[65] It has previously been reported that EBs formation prior to chemically-induced osteogenic differentiation is not necessary and may, in fact, hamper osteogenic potential of hPSCs.[66, 67] Besides, EBs displayed outgrowth on all surfaces but had already formed cell-cell contacts thus reducing cell-substrate contact, so it is a less-than-ideal model for investigation of cell-substrate influence.[68] Without EBs formation step, biomineralized PEGDA-co-A6ACA matrices[1] and osteomimetic PLGA scaffolds[69] were recently developed to direct osteogenic differentiation of hESCs. However, these developments required the materials to be pre-coated with Matrigel and ECM protein to promote initial attachment of hPSCs. Although there are a few work on osteoblastic differentiation of mouse iPSCs on the fibrous scaffolds surface, but studies focusing on human

iPSCs is missing. We try to investigate and verify that hPSCs can achieve high yield differentiation into osteoblastic cells on the prepared peptide-decorated nanofibrous niche. Simultaneously, classic β-glycerophosphate (β-GP), ascorbic acid (AA) and dexamethasone as effective chemical-induced factors was added into osteogenic medium to trigger the mineralization of hPSCs. In the present work, hPSCs were directly potentiated to osteogenic commitment on our peptides-decorated surface without EBs process and Matrigel/ECM coating (i.e., under chemically defined conditions) coupled with biochemical and biophysical cues, which could provide an efficient and safe microenvironment for bone tissue engineering. Furthermore, the degree of orientation and size of nanofibers were pointed out to have a powerful impact on cell differentiation, hence, future work should include the comprehensive exploration of physical factors including orientation degree and size of nanofibers in the influence on the ostegenic differenation of hPSCs.

4. CONCLUSION

In this study, we demonstrated a facile and cost-effective approach to produce a novel peptide-decorated nanofibour niche through combining electrostatic spinning of PCL with VN peptide conjugation to modulate hPSC differentiation towards osteoblastic phenotype. The modified nanofiber surfaces could support the proliferation and retain the pluripotency of hiPSCs and hESCs in a fully-defined basal media (mTeSR^{TM}1). More interestingly, the celluar morphology observation, ALP activity assessment, and RT-PCR analysis combined with immunofluorescence results demonstrated that hPSCs incubated on the peptide-decorated micromilieu underwent enhanced osteogenic conversion *in vitro* without induction of differentiation by EB formation. The osteogenic culture system without Matrigel coating has

merits of eradicating risks of viral and microbial contamination picked up from animal-derived proteins. Therefore, this chemically-defined and safe 3D fibrous niche, that supports the whole process from hPSCs clture to osteogenic commitment, has promising potential for bone regenerative medicine and tissue engineering.

ASSOCIATED CONTENT

Supporting Information

Figures S1-S4 and Tables S1-S2. This material is available free of charge *via* the Internet at http://pubs.acs.org

AUTHOR INFORMATION

Corresponding Author

*Dr. Yi Deng

School of Chemical Engineering, Sichuan University,

No.24 South Section 1, Yihuan Road, Chengdu 610065, China,

Email: 18210357357@163.com.

*Prof. Shicheng Wei

School and Hospital of Stomatology, Peking University,

No. 22 South Street, Zhongguancun, Haidian District, Beijing, 100081, China,

Email: weishicheng991@163.com.

Author Contributions

The manuscript was written through contributions of all authors. All authors have given approval to the final version of the manuscript.

Notes

The authors declare no competing financial interest.

ACKNOWLEDGMENT

This work was funded by the National Natural Science Foundation of China (No. 81371697, 81571824), Peking University's 985 Grant, and the financial support from scientific research foundation of Sichuan University.

REFERENCES

(1) Kang, H.; Wen, C.; Hwang, Y.; Shih, Y. R.; Kar, M.; Seo, S. W.; Varghese, S. *J. Mater. Chem. B* **2014**, *2*, 5676-5688.

(2) Nelson, T. J.; Martinezfernandez, A.; Terzic, A. *Nat. Rev. Cardiol.* **2010**, *7*, 700-710.

(3) Takahashi, K.; Yamanaka, S. *Cell* **2006**, *126*, 663-676.

(4) Kim, J. B.; Zaehres, H.; Wu, G.; Gentile, L.; Ko, K.; Sebastiano, V.; Araúzobravo, M. J.; Ruau, D.; Han, D. W.; Zenke, M. *Nature* **2008**, *454*, 646-650.

(5) Hughes, C. S.; Postovit, L. M.; Lajoie, G. A. *Proteomics* **2010**, *10*, 1886-1890.

(6) Deng, Y.; Zhang, X.; Zhao, X.; Li, Q.; Ye, Z.; Li, Z.; Liu, Y.; Zhou, Y.; Ma, H.; Pan, G. *Acta Biomater.* **2013**, *9*, 8840-8850.

(7) Saha, K.; Mei, Y.; Reisterer, C. M.; Pyzocha, N. K.; Yang, J.; Muffat, J.; Davies, M. C.; Alexander, M. R.; Langer, R.; Anderson, D. G. *P. Natl. Acad. Sci. USA* **2011**, *108*, 18714-18719.

(8) Rowland, T. J.; Miller LMBlaschke, A. J.; Doss, E. L.; Bonham, A. J.; Hikita, S. T.; Johnson, L. V.; Clegg, D. O. *Stem Cells Dev.* **2010**, *19*, 1231-1240.

(9) Rodin, S.; Domogatskaya, A.; Strm, S.; Hansson, E. M.; Chien, K. R.; Inzunza, J.; Hovatta, O.; Tryggvason, K. *Nat. Biotechnol.* **2010**, *28*, 611-615.

(10) Liu, L.; Yoshioka, M.; Nakajima, M.; Ogasawara, A.; Liu, J.; Hasegawa, K.; Li, S.; Zou, J.; Nakatsuji, N.; Kamei, K. I. *Biomaterials* **2014**, *35*, 6259-6267.

(11) Brafman, D. A.; Chang, C. W.; Fernandez, A.; Willert, K.; Varghese, S.; Shu, C. *Biomaterials* **2010**, *31*, 9135-9144.

(12) Kang, H.; Shih, Y. R. V.; Hwang, Y.; Wen, C.; Rao, V.; Seo, T.; Varghese, S. *Acta Biomater.* **2014**, *10*, 4961-4970.

(13) Xu, C.; Inai, R.; Kotaki, M.; Ramakrishna, S. *Tissue Eng.* **2004**, *10*, 1160-1168.

(14) Wang, S.; Zhong, S.; Lim, C. T.; Nie, H. *J. Mater. Chem. B* **2015**, *3*, 3358-3366.

(15) Ko, E. K.; Jeong, S. I.; Rim, N. G.; Lee, Y. M.; Shin, H.; Lee, B. K. *Tissue Eng. A* **2008**, *14*, 2105-2119.

(16) Ardeshirylajimi, A.; Hosseinkhani, S.; Parivar, K.; Yaghmaie, P.; Soleimani, M. *Mol. Biol. Rep.* **2013**, *40*, 4287-4294.

(17) Ravichandran, R.; Venugopal, J. R.; Sundarrajan, S.; Mukherjee, S.; Ramakrishna, S. *Biomaterials* **2012**, *33*, 846-855.

(18) Ho, M. H.; Liao, M. H.; Lin, Y. L.; Lai, C. H.; Lin, P.; Chen, R. M. *Int. J. Nanomed.* **2014**, *9*, 4293-4304.

(19) Higuchi, A.; Kumar, S. S.; Ling, Q-D.; Alarfaj, A. A.; Munusamy, M. A.; Murugan, K.; Hsu, S-T.; Benelli, G.; Umezawa, A. *Prog. Polym. Sci.* **2016**, http://dx.doi.org/10.1016/j.progpolymsci.2016.09.002.

(20) Higuchi, A.; Ling, Q. D.; Kumar, S. S.; Munusamy, M.; Alarfajj, A. A.; Umezawa, A.; Wu, G. J. *Prog. Polym. Sci.* **2014,** *39*, 1348-1374.

(21) Dong, X.; Li, H.; Zhou, Y.; Ou, L.; Cao, J.; Chang, J. *J. Mater. Chem. B* **2016**, *4*, 2369-2376.

(22) Higuchi, A.; Ling, Q. D.; Kumar, S. S.; Chang, Y.; Alarfaj, A. A.; Munusamy, M. A.; Murugan, K.; Hsu, S. T.; Umezawa, A. *J. Mater. Chem. B* **2015**, *3*, 8032-8058.

(23) Cipitria, A. *J. Mater. Chem.* **2011**, *21*, 9419-9453.

(24) Villa-Diaz, L. G.; Nandivada, H.; Ding, J.; Nogueira-De-Souza, N. C.; Krebsbach, P. H.; O'Shea, K. S.; Lahann, J.; Smith, G. D. *Nat. Biotechnol.* **2010**, *28*, 581-583.

(25) Bhattacharya, D.; Das, M.; Mishra, D.; Banerjee, I.; Sahu, S. K.; Maiti, T. K.; Pramanik, P. *Nanoscale* **2011**, *3*, 1653-1662.

(26) Chen, R. N.; Wang, G. M.; Chen, C. H.; Ho, H. O.; Sheu, M. T. *Biomacromolecules* **2006**, *7*, 1058-1064.

(27) Shi, Z.; Neoh, K. G.; Kang, E. T.; Poh, C. K.; Wang, W. *Biomacromolecules* **2009**, *10*, 1603-1611.

(28) Budiraharjo, R.; Neoh, K. G.; Kang, E. T. *J. Colloid Interf. Sci.* **2012**, *366*, 224-232.

(29) Danesin, R.; Brun, P.; Roso, M.; Delaunay, F.; Samouillan, V.; Brunelli, K.; Iucci, G.; Ghezzo, F.; Modesti, M.; Castagliuolo, I. *Bone* **2012**, *51*, 851-859.

(30) Chen, S. C.; Wu, Y. C.; Mi, F. L.; Lin, Y. H.; Yu, L. C.; Sung, H. W. *J. Control. Release* **2004**, *96*, 285-300.

(31) Nandakumar, A.; Tahmasebi, B. Z.; Santos, D.; Mentink, A.; Auffermann, N.; Van, d. W. K.; Bennink, M.; Moroni, L.; Van, B. C.; Habibovic, P. *Biofabrication* **2013**, *5*, 015006.

(32) Wang, H.; Kwok, D. T. K.; Xu, M.; Shi, H.; Wu, Z.; Zhang, W.; Chu, P. K. *Adv. Mater.* **2012**, *24*, 3315-3324.

(33) Wilkinson, A.; Hewitt, R. N.; Mcnamara, L. E.; Mccloy, D.; Meek, R. M. D.; Dalby, M. J. *Acta Biomater.* **2011**, 7, 2919-2925.

(34) Azeem, A.; English, A.; Kumar, P.; Satyam, A.; Biggs, M.; Jones, E.; Tripathi, B.; Basu, N.; Henkel, J.; Vaquette, C. *Nanomedicine* **2015**, 10, (5), 693-711.

(35) Xu, A.; Liu, X.; Xiang, G.; Feng, D.; Yi, D.; Wei, S. *Mat. Sci. Eng. C* **2015**, *48*, 592-598.

(36) Park, H. J.; Yang, K.; Kim, M. J.; Jang, J.; Lee, M.; Kim, D. W.; Lee, H.; Cho, S. W. *Biomaterials* **2015**, *50*, 127-139.

(37) Gao, X.; Zhang, X.; Song, J.; Xu, X.; Xu, A.; Wang, M.; Xie, B.; Huang, E.; Deng, F.; Wei, S. *Inter. J. Nanomed.* **2015**, *10*, 7109-7128.

(38) Jing, X.; Mi, H. Y.; Peng, J.; Peng, X. F.; Turng, L. S. *Carbohyd. Polym.* **2015**, *117*, 941-949.

(39) Hu, B. Y.; Weick, J. P.; Yu, J.; Ma, L. X.; Zhang, X. Q.; Thomson, J. A.; Zhang, S. C. *P. Natl. Acad. Sci. USA* **2010**, *107*, 4335-4340.

(40) Song, Z.; Cai, J.; Liu, Y; Zhao, D.; Yong, J.; Duo, S.; Song, X.; Guo, Y.; Zhao, Y.; Qin, H.; Yin, X.; Wu, C.; Che, J.; Lu, S.; Ding, M.; Deng, H. *Cell Research* **2009**, *19*, 1233-1242.

(41) Chen, Y-F.; Tseng, C-Y.; Wang, H-W.; Kuo, H-C.; Yang V. W.; Lee, O. K. *Hepatology*, **2012**, *55*, 1193-1203.

(42) Lian, X.; Hsiao, C.; Wilson, G.; Zhu, K.; Hazeltine, L. B.; Azarin, S. M.; Raval, K. K.; Zhang, J.; Kamp, T. J.; Palecek, S. P. *P. Natl. Acad. Sci. USA*, **2012**, *109*, 4933-4942.

(43) Burridge, P.; Keller, G.; Gold, J.; Wu, J. *Cell Stem Cell* **2012**, *10*, 16-28.

(44) Charles, A. E. IV; Phillips, B.; Mcguire, M.; Barringer, J.; Valli, H.; Hermann, B.; Simerly, C.; Rajkovic, A.; Miki, T.; Orwig, K. *Cell Reports* **2011**, *2*, 440-446.

(45) Li, Y. J.; Chung, E. H.; Rodriguez, R. T. *J. Biomed. Mater. Res. A* **2006**, *79A*, 1-5.

(46) Lu, H. F.; Narayanan, K.; Lim, S.-X.; Gao, S.; Leong, M. F.; Wan, A. C. A. *Biomaterials* **2012**, *33*, 2419-2430.

(47) Reubinoff, B. E.; Pera, M. F.; Fong, C. Y.; Trounson, A.; Bongso, A. *Nat. Biotechnol.* **2000**, *18*, 399-404.

(48) Schopperle, W. M.; Dewolf, W. C. *Stem Cells* **2007**, *25*, 723-730.

(49) Christopherson, G. T.; Song, H.; Mao, H. Q. *Biomaterials* **2009**, *30*, 556-564.

(50) Kaur, G.; Valarmathi, M. T.; Potts, J. D.; Wang, Q. *Biomaterials* **2008**, *29*, 4074-81.

(51) Liu, W.; Lipner, J.; Xie, J.; Manning, C. N.; Thomopoulos, S.; Xia, Y. *ACS Appl. Mater. Inter.* **2011**, *6*, 2842-2849.

(52) Yin, L.; Cheng, W.; Qin, Z.; Yu, H.; Yu, Z.; Zhong, M.; Sun, K.; Zhang, W. *Stem Cells Int.* **2015**, *2015*, 1-9.

(53) Sachar, A.; Strom, T. A.; Serrano, M. J.; Benson, M. D.; Opperman, L. A.; Svoboda, K. K. H.; Liu, X. *J. Biomed. Mater. Res. A* **2012**, *100*, 3029-3041.

(54) Horii, A.; Wang, X.; Gelain, F.; Zhang, S. *Plos One* **2007**, *2*, e190.

(55) Lee, Y. J.; Lee, J. H.; Cho, H. J.; Kim, H. K.; Yoon, T. R.; Shin, H. *Biomaterials* **2013**, *34*, 5059-69.

(56) Frantz, C.; Stewart, K. M.; Weaver, V. M. *J. Cell Sci.* **2010**, *123*, 4195-200.

(57) Lahiji, A.; Sohrabi, A.; Hungerford, D. S.; Frondoza, C. G. *J. Biomed. Mater. Res.* **2000,** *51*, 586-595.

(58) Chowdhury, F.; Li, Y.; Poh, Y. C.; Yokohama-Tamaki, T.; Wang, N.; Tanaka, T. S. *Plos One* **2010,** *5*, e15655.

(59) Lim, S. H.; Liu, X. Y.; Song, H.; Yarema, K. J.; Mao, H. Q. *Biomaterials* **2010**, *31*, 9031-9039.

(60) Wang, Y.; Gao, R.; Wang, P. P.; Jian, J.; Jiang, X. L.; Yan, C.; Lin, X.; Wu, L.; Chen, G. Q.; Wu, Q. *Biomaterials* **2012**, *33*, 485-493.

(61) Zhu, H.; Cao, B.; Zhen, Z.; Laxmi, A. A.; Li, D.; Liu, S.; Mao, C. *Biomaterials* **2011**, *32*, 4744-4752.

(62) Hu, J.; Liu, X.; Ma, P. X. *Biomaterials* **2008**, *29*, 3815-3821.

(63) Liu, W.; Wei, Y.; Zhang, X.; Xu, M.; Yang, X.; Deng, X. *ACS Nano* **2013**, *7*, 6928-6938.

(64) Smith, L. A.; Liu, X.; Jiang, H.; Ma, P. X. *Biomaterials* **2010,** *31*, 5526-5535.

(65) Dang, S. M.; Kyba, M.; Perlingeiro, R.; Daley, G. Q.; Zandstra, P. W. *Biotechnol. Bioeng.* **2002,** *78*, 442-453.

(66) Karp, J. M.; Ferreira, L. S.; Khademhosseini, A.; Kwon, A. H.; Yeh, J.; Langer, R. S. *Stem Cells* **2006,** *24*, 835-843.

(67) Kärner, E.; Unger, C.; Sloan, A. J.; Ahrlundrichter, L.; Sugars, R. V.; Wendel, M. *Stem Cells Dev.* **2007,** *16*, 39-52.

(68) Kingham, E.; White, K.; Gadegaard, N.; Dalby, M. J.; Oreffo, R. O. C. *Small* **2013**, *9*, 2140-51.

(69) Rutledge, K.; Cheng, Q.; Pryzhkova, M.; Harris, G. M.; Jabbarzadeh, E. *Tissue Eng. C*, **2014**, *20*, 865-874.

Captions of Figures and Tables

Fig. 1. Schematic illustration of the fabrication of peptide-decorated nanofibrous microenvironment, and *in vitro* culture and directed osteogenic induction of hPSCs on the fibrous niche.

Fig. 2. ATR-FT-IR spectra (a), water contact angles and corresponding surface energy (b) of the pristine and functionalized PCL nanofibrous scaffolds (CMC-PCL, and pep-CMC-PCL).

Fig. 3. XPS survey scan spectra: XPS wide spectra (a); high-resolution spectra of carbon peaks (C 1s) for the pristine PCL (b), CMC-PCL (c) and pep-CMC-PCL (c).

Fig. 4. SEM and corresponding AFM images of the (a) pristine PCL, (b) CMC-coated PCL and (c) peptide-decorated PCL nanofibers samples.

Fig. 5. The proliferation of hiPSCs (a) and hESCs (b) on the surface of peptide-decorated PCL nanofibrous scaffold with different culture time.

Fig. 6. SEM observation of adhering hPSCs on the peptide-decorated nanofibers from 1 day to 5 days.

Fig. 7. Fluorescence micrographs of colonies of hPSCs cultured on the peptide-decorated substrate at 1 day and 3 days in mTeSR™1 media visualized by laser confocal microscopy, showing expression of hPSC markers: Oct-4, Tra-1-60, SSEA-3 and SSEA-4.

Fig. 8. hiPSCs (a) and hESCs (b) morphology changes during osteo-differentiation on peptide-decorated PCL nanofibers under osteogenic inducing medium at various culture times. Red arrows point to the filopodia of the differentiated cells adhered to the substrate. The scale bar indicates 50 μm.

Fig. 9. ALP activity of hiPSCs (a) and hESCs (b) cultured on pep-CMC-PCL nanofibers and pep-CMC-glass surfaces. *represents $p < 0.05$ between groups.

Fig. 10. Real-time PCR detection of osteogenesis-related gene expression (Runx2, ALP, Col1a1, and OCN) of hiPSCs and hESCs incubated on the two peptide-decorated samples at Day 7, 14 and 21. *represents $p< 0.05$ compared with pep-CMC-glass, and **represents $p< 0.01$ compared with pep-CMC-glass.

Fig. 11. Immunofluorescent images of Col1a1 (green), OPN (red), OCN (red), and cytoskeleton (green) on the peptide-decorated nanofiber substrates at Day 21. Col1a1 and cytoskeleton were labeled by green fluorescence, whereas OPN and OCN were marked by green fluorescence. Nanofiber were visualized to blue color at 488 nm excitation wavelength.

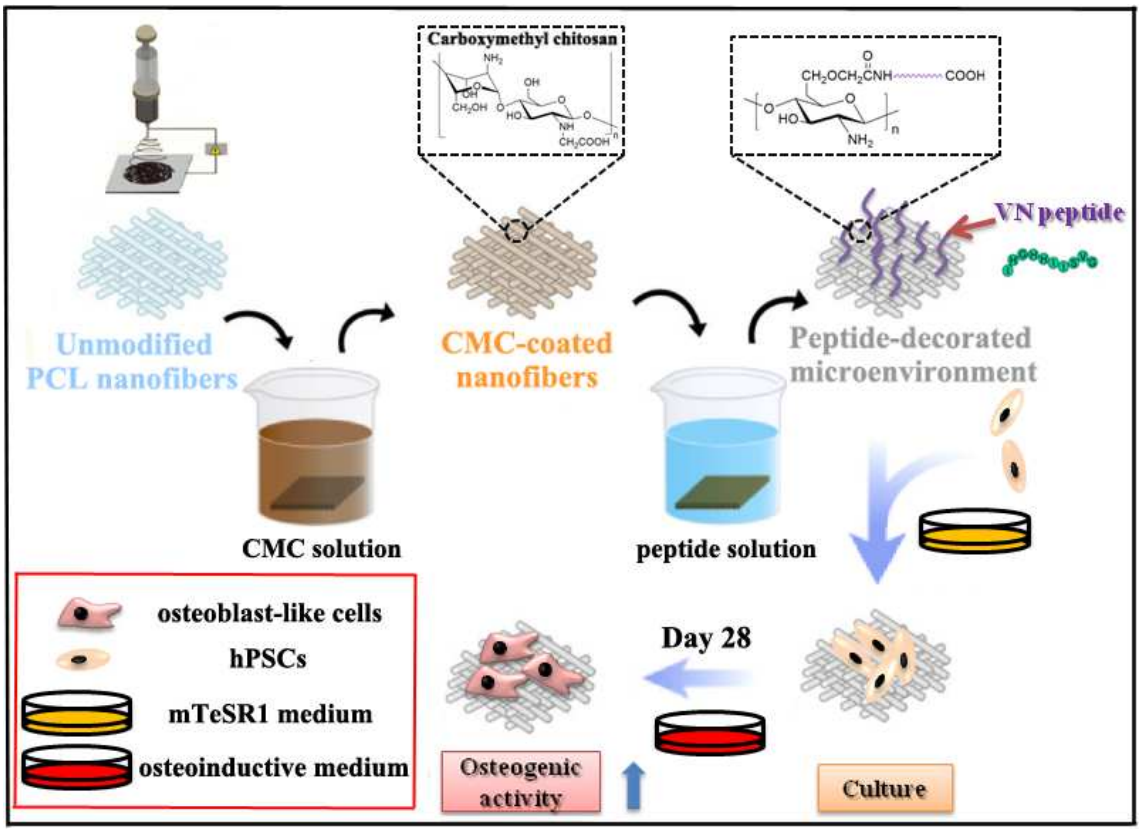

Fig. 1. Schematic illustration of the fabrication of peptide-decorated nanofibrous microenvironment, and *in vitro* culture and directed osteogenic induction of hPSCs on the fibrous niche.

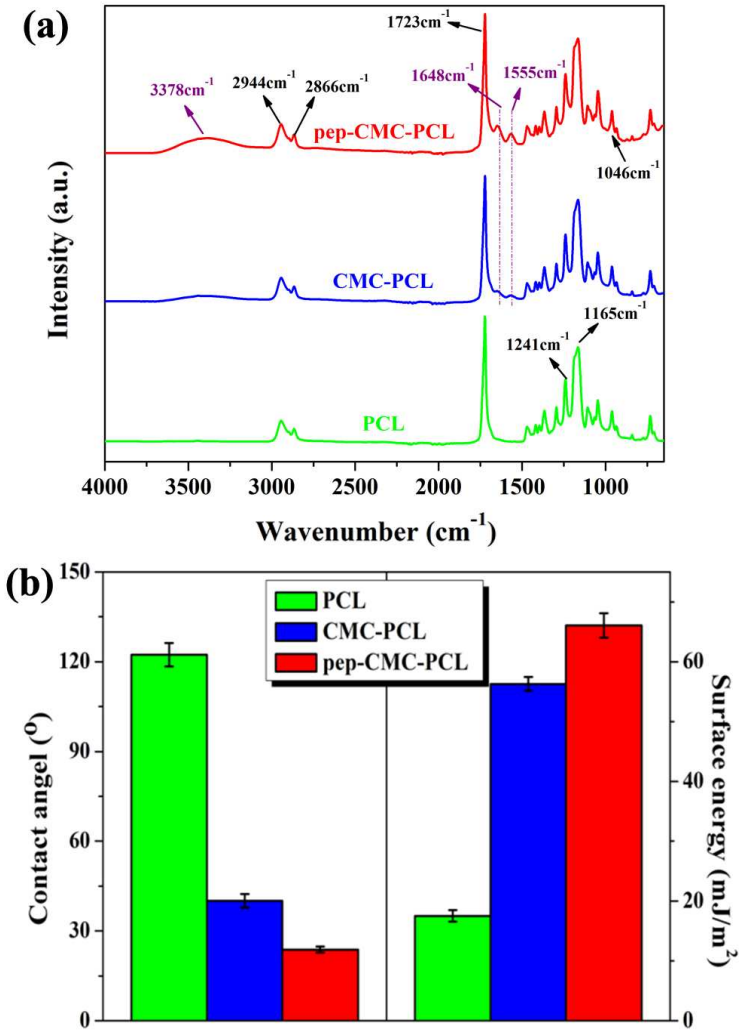

Fig. 2. ATR-FT-IR spectra (a), water contact angles and corresponding surface energy (b) of the pristine and functionalized PCL nanofibrous scaffolds (CMC-PCL, and pep-CMC-PCL).

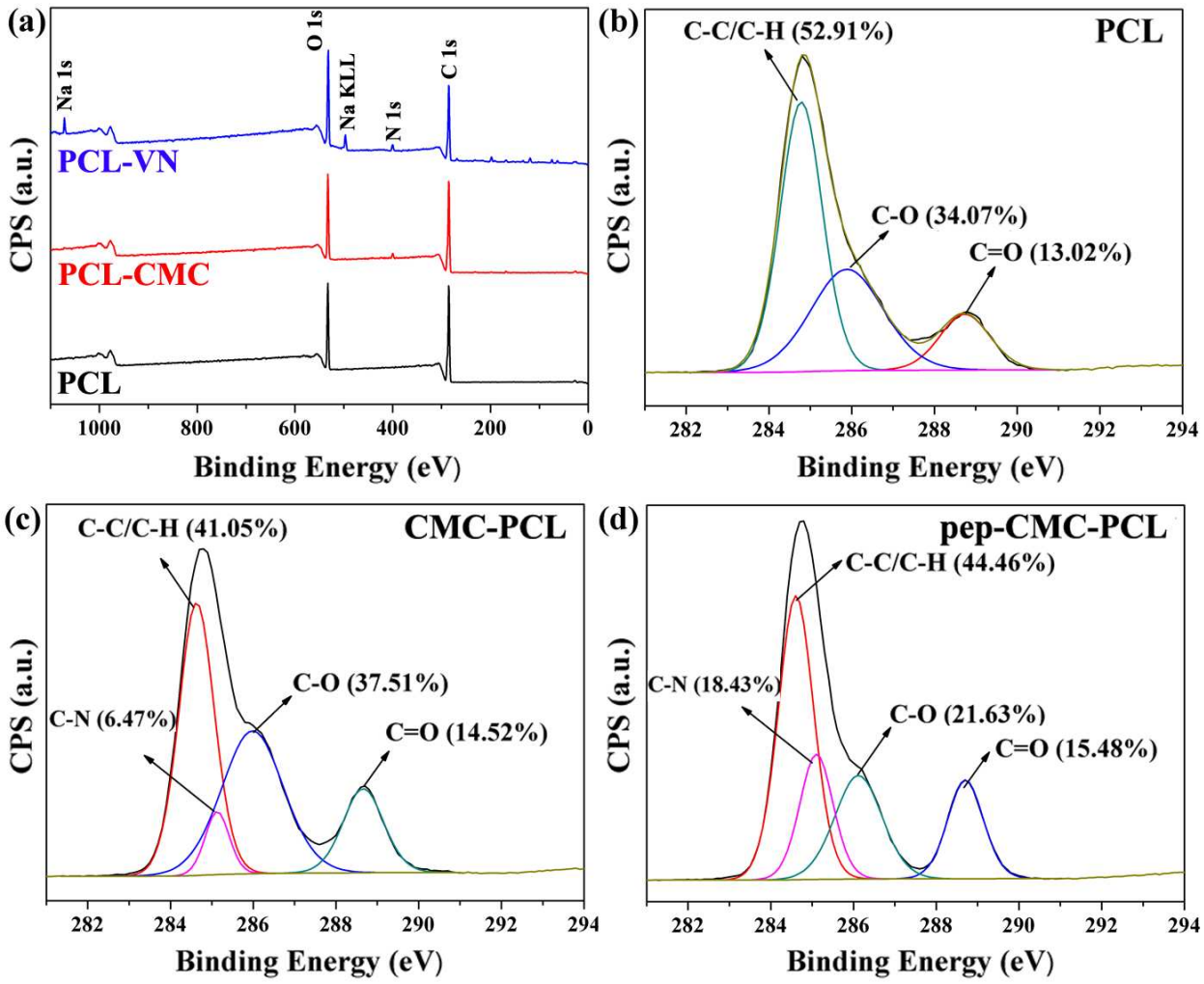

Fig. 3. XPS survey scan spectra: XPS wide spectra (a); high-resolution spectra of carbon peaks (C 1s) for the pristine PCL (b), CMC-PCL (c) and pep-CMC-PCL (c).

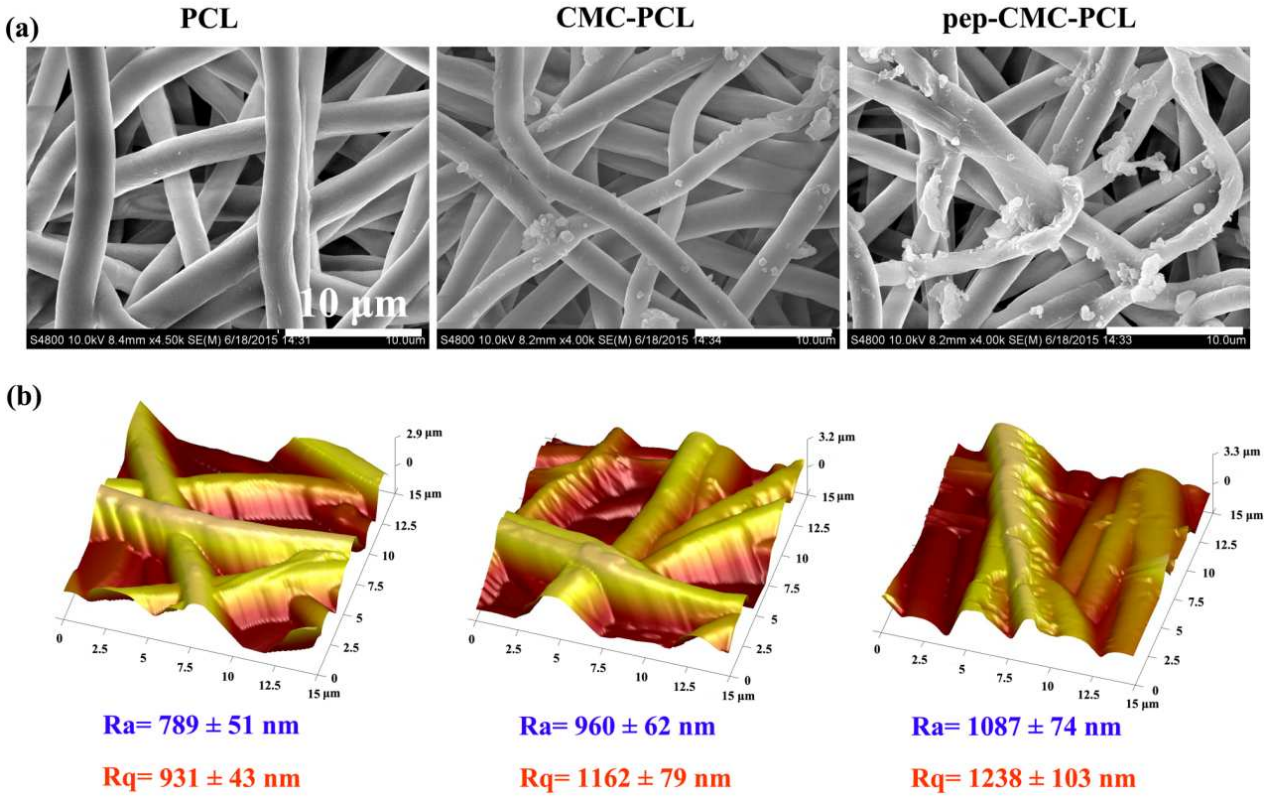

Fig. 4. SEM and corresponding AFM images of the (a) pristine PCL, (b) CMC-coated PCL and (c) peptide-decorated PCL nanofibers samples.

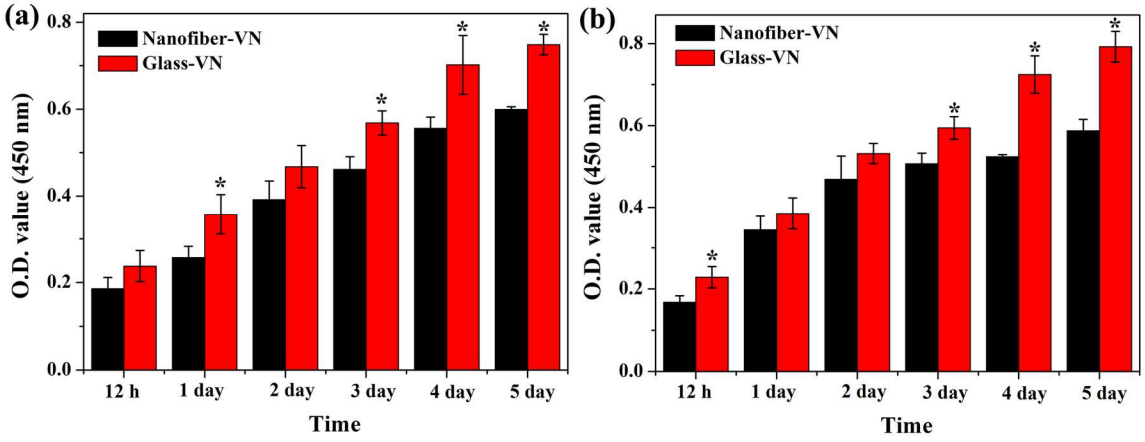

Fig. 5. The proliferation of hiPSCs (a) and hESCs (b) on the surface of peptide-decorated PCL nanofibrous scaffold with different culture time.

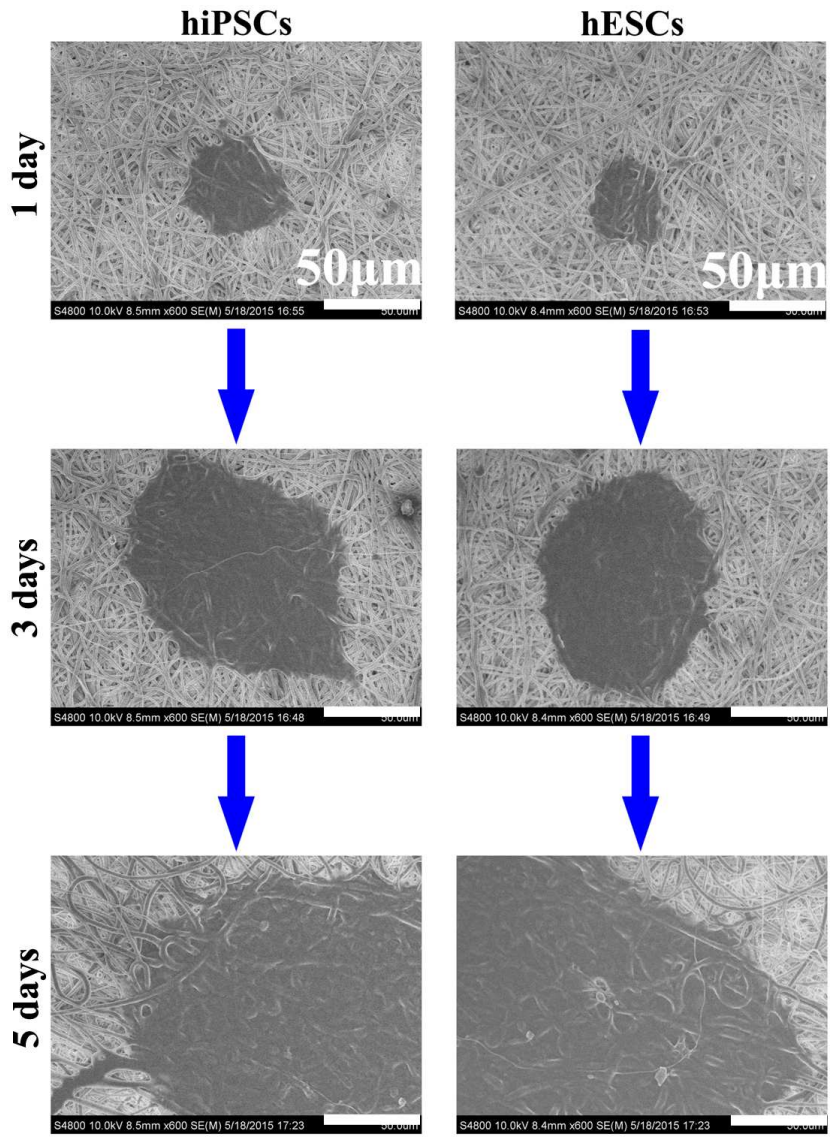

Fig. 6. SEM observation of adhering hPSCs on the peptide-decorated nanofibers from 1 day to 5 days.

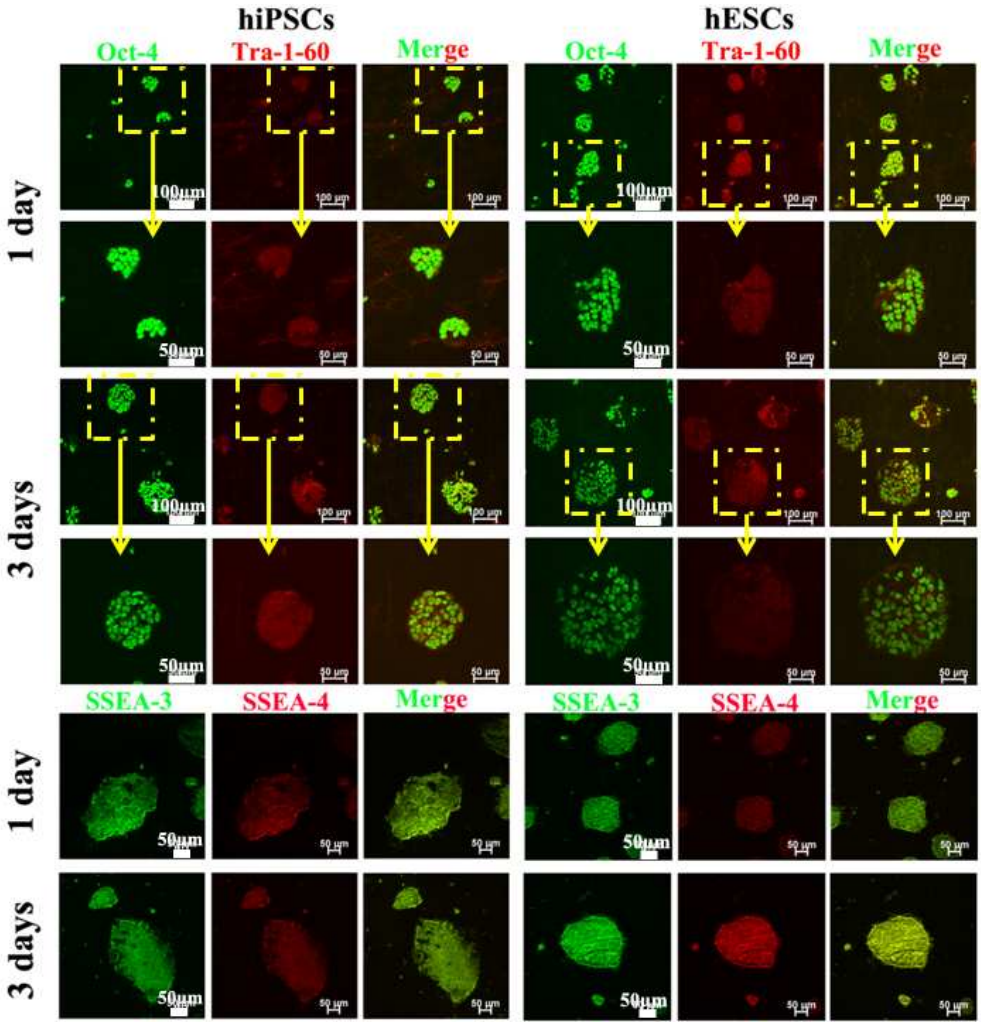

Fig. 7. Fluorescence micrographs of colonies of hPSCs cultured on the peptide-decorated substrate at 1 day and 3 days in mTeSR™1 media visualized by laser confocal microscopy, showing expression of hPSC markers: Oct-4, Tra-1-60, SSEA-3 and SSEA-4.

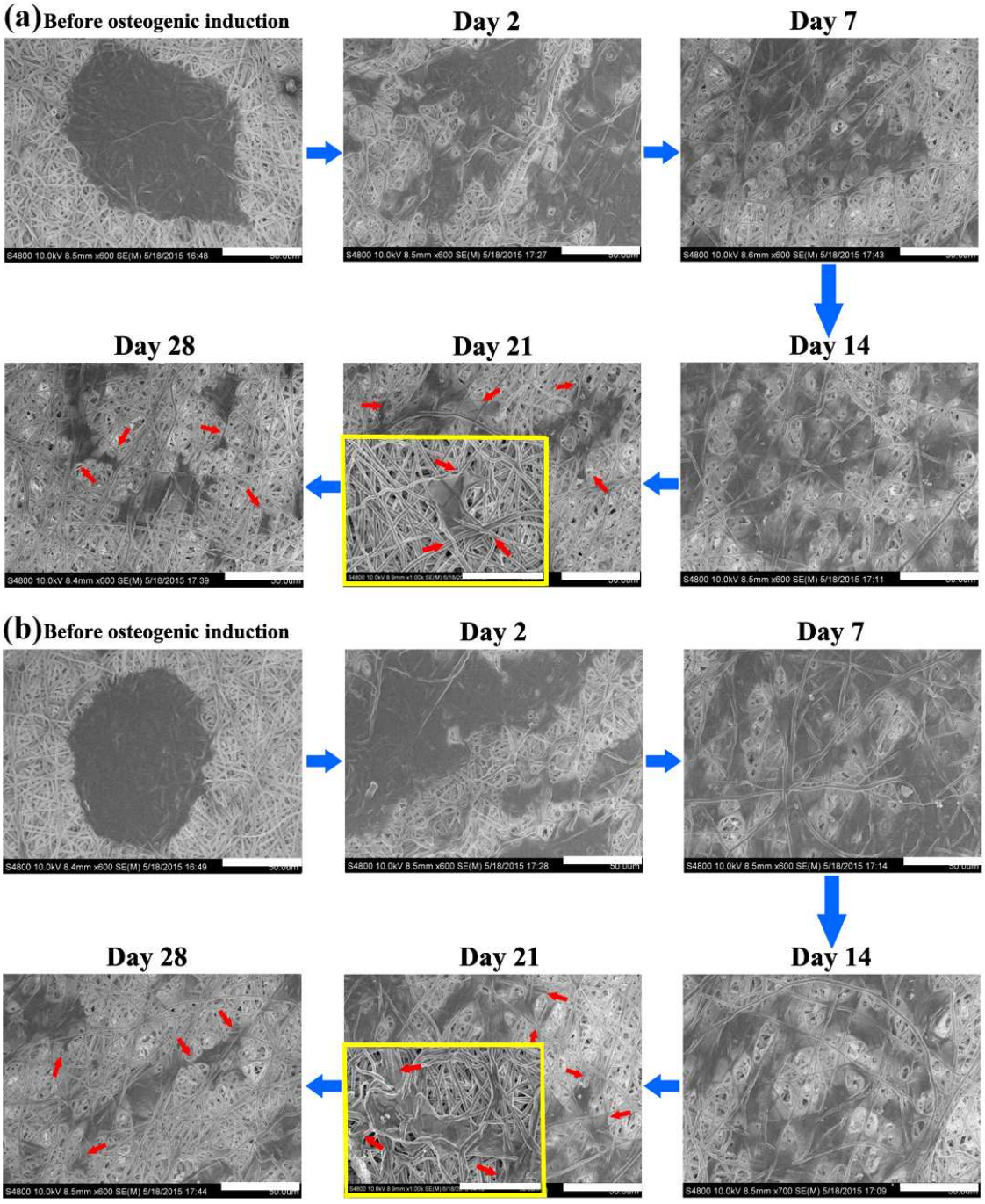

Fig. 8. hiPSCs (a) and hESCs (b) morphology changes during osteo-differentiation on peptide-decorated PCL nanofibers under osteogenic inducing medium at various culture times. Red arrows point to the filopodia of the differentiated cells adhered to the substrate. The scale bar indicates 50 µm.

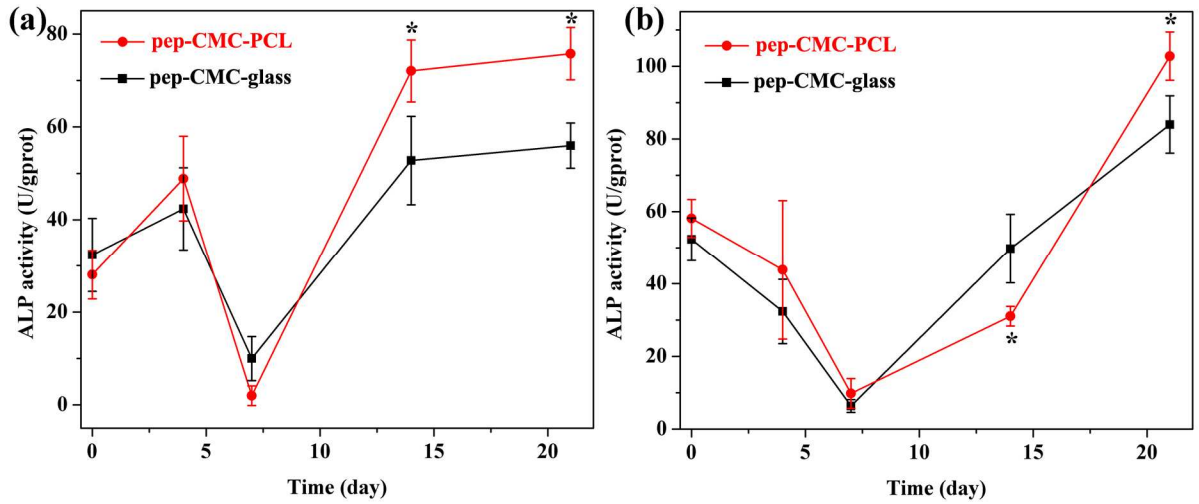

Fig. 9. ALP activity of hiPSCs (a) and hESCs (b) cultured on pep-CMC-PCL nanofibers and pep-CMC-glass surfaces. *represents $p < 0.05$ between groups.

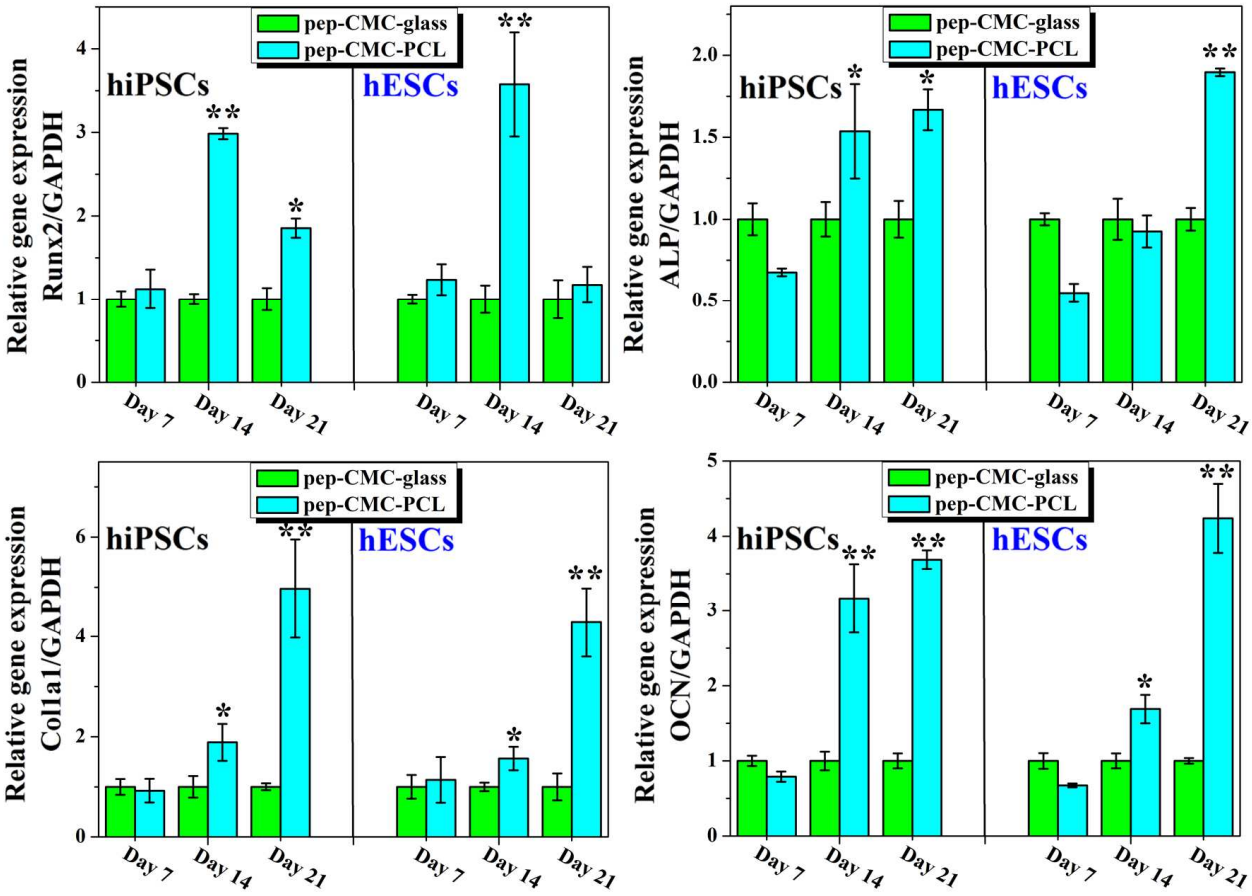

Fig. 10. Real-time PCR detection of osteogenesis-related gene expression (Runx2, ALP, Col1a1, and OCN) of hiPSCs and hESCs incubated on the two peptide-decorated samples at Day 7, 14 and 21. *represents $p< 0.05$ compared with pep-CMC-glass, and **represents $p< 0.01$ compared with pep-CMC-glass.

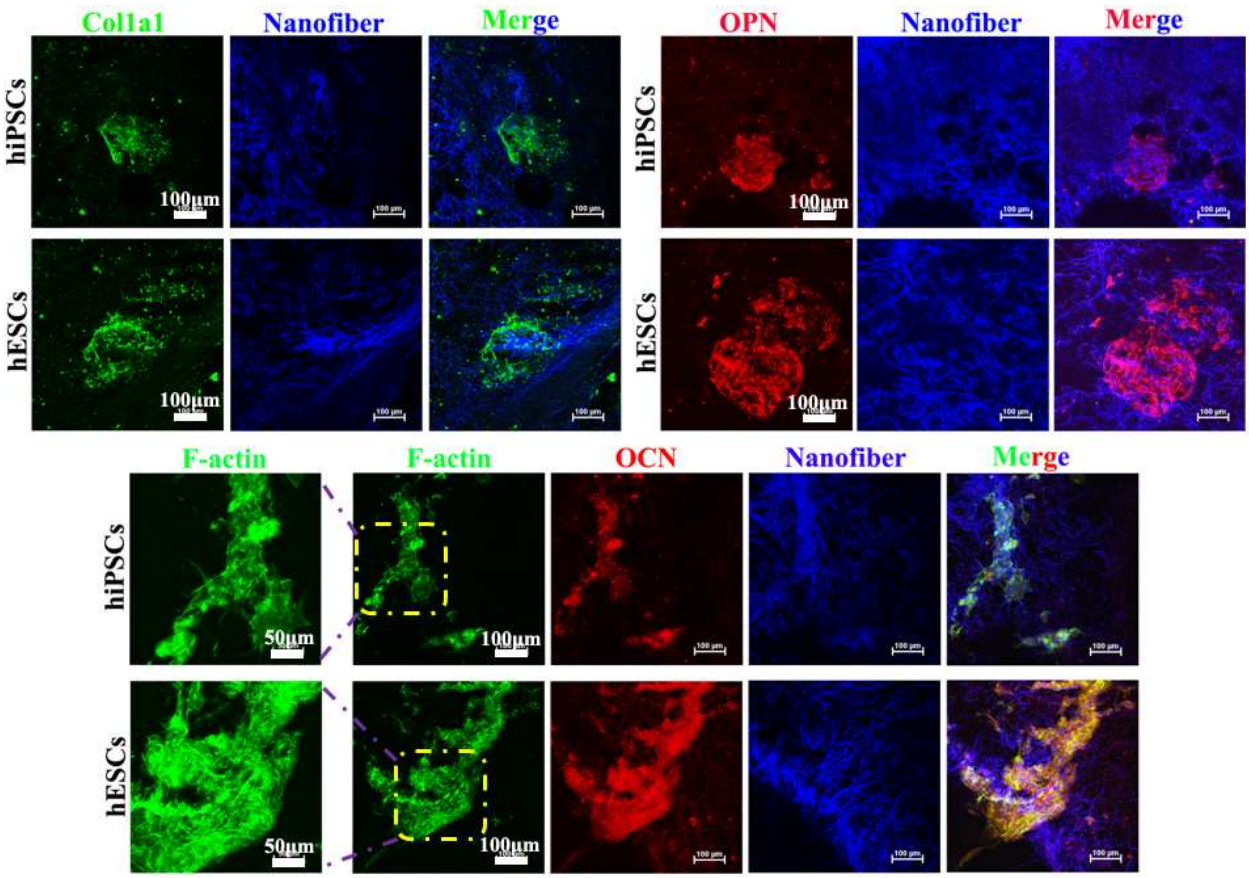

Fig. 11. Immunofluorescent images of Col1a1 (green), OPN (red), OCN (red), and cytoskeleton (green) on the peptide-decorated nanofiber substrates at Day 21. Col1a1 and cytoskeleton were labeled by green fluorescence, whereas OPN and OCN were marked by green fluorescence. Nanofiber were visualized to blue color at 488 nm excitation wavelength.

Table of Contents Graphic

For Table of Contents Use Only

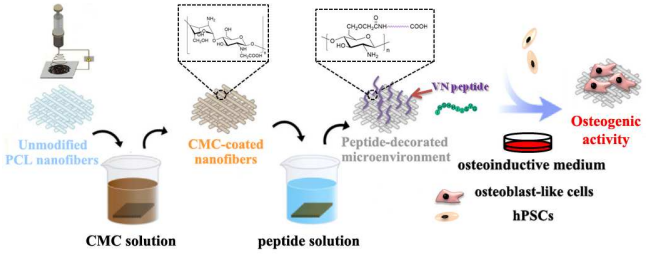

Peptide-decorated nanofibrous niche augments in vitro directed osteogenic conversion of human pluripotent stem cells

Yi Deng, Yuanyi Yang, Shicheng Wei